NIH Public Access
Author Manuscript
J Mater Chem B Mater Biol Med. Author manuscript; available in PMC 2015 January 01.

Published in final edited form as:
J Mater Chem B Mater Biol Med. 2014 ; 2(43): 7534–7543. doi:10.1039/C4TB01195C.

Gold Nanopopcorn Attached Single-Walled Carbon Nanotube Hybrid for Rapid Detection and Killing of Bacteria

Thomas. J. Ondera and **Ashton. T. Hamme II**
Department of Chemistry and Biochemistry, Jackson State University, 1400 J R Lynch street, Jackson, MS 39217, USA.

Ashton. T. Hamme: ashton.t.hamme@jsums.edu

Abstract

We report a strategy to fabricate a rapid and stable surface-enhanced Raman scattering (SERS)-based hybrid nanomaterial using gold nanopopcorns attached single-walled carbon nanotubes (AuNP@f_3-SWCNTs) for label-free detection and photothermal killing of bacteria. Herein, previously ester-functionalized single-walled carbon nanotubes (f_1-SWCNTs) undergo 1,3-dipolar cycloaddition reaction with *in-situ* generated nitrile imine under Microwave (MW) irradiation to form a doubly ester terminated SWCNTs cycloadduct (f_2-SWCNTs). The ester terminals are further modified with 4-aminothiophenol (4-ATP) under MW-irradiation to form thiol-terminated SWCNTs templates (f_3-SWCNTs) that allow gold nanopopcorns (AuNPs) to covalently and uniformly attach at a minimum inter-particle distance thus yielding a hybrid nanomaterial (AuNP@f_3-SWCNT) with good aqueous stability and abundant 'hotspots'. Consequently, monoclonal *E. coli* antibody-conjugated bioassays fabricated with our AuNP@f_3-SWCNT substrates (mAb-AuNP@f_3-SWCNT) rapidly detect *E. coli* in water with good selectivity and impressive SERS sensitivity. The detection limit of *E. coli 49979*, selected as a model to establish proof of principle, was found to be 1.0×10^2 CFU/mL. Furthermore, the AuNP@f_3-SWCNT hybrid nanomaterial offers impressive photothermal pathogen killing effects. The synergy-type enhancement effect arising from the inherent noble properties of the respective components of the hybrid nanomaterial indicate that our AuNP@f_3-SWCNT has the potential for further application in multiplex detection in samples.

1 Introduction

The detection, identification and quantification of microbes have become a key concern in water safety, food safety, biodefense, diagnostics and drug discovery research. Detection of microbes is usually realized by traditional methods through culturing, enrichment and identification steps. The traditional methods are time consuming and laborious. Modern state-of-the art techniques such as Polymerase Chain reaction (PCR), though very rapid and sensitive, are very susceptible to contamination resulting in false positive results.

This journal is © The Royal Society of Chemistry 2014
Correspondence to: Ashton. T. Hamme, II, ashton.t.hamme@jsums.edu.

NIH-PA Author Manuscript
NIH-PA Author Manuscript
NIH-PA Author Manuscript

NIH-PA Author Manuscript

NIH-PA Author Manuscript

NIH-PA Author Manuscript

The process of labelling ELISA samples is usually time consuming and quite costly due to requirement for extra labelled antibodies. Significant research efforts have focused on developing cheap, easy to use, rapid and ultrasensitive bioassays to detect water-borne pathogens. Approaches such as fluorescence, potentiometric, colorimetric, inductive coupled plasma (ICP), mass spectrometry (MS), flow cytometer techniques, among others, have been reported.[1–7] However, these suffer from several constraints. Even though fluorescence is very sensitive, this technique is inherently limited by the poor photostability of the organic dyes used as labels and hence less than ideal for optical detection systems. Potentiometric measurements are limited by their temperature dependence and the fact that adsorption of solution components on membrane surfaces can affect the nature of the charge transfer and hence may yield inaccurate results. Colorimetric methods are not entirely satisfactory because, at low concentrations, the colour changes are barely noticeable to the eye. ICP, MS, and flow cytometer techniques often require a combination of other methods and elaborate support facilities to detect microorganisms.[1–7]

SERS-based nanotechnology is emerging as a promising technique that can be used to address these challenges.[8–23] SERS-based bioassays have been developed from metal colloids,[8–11,14–16] carbon nanotubes templates[21] and self-assembled membranes (SAMs)[13,17] by using various techniques with the goal of increasing sensitivity and accuracy. However, most of these still face the challenge of low reproducibility and poor stability. Several groups have reported strategies to fabricate SERS substrates that have exhibited promising results over the colloidal metal nanostructures or the lithographically fabricated substrates.[21–23]

Single-walled carbon nanotubes (SWCNTs), as AuNP supporters, have the potential for building practical hybrid SERS substrates because they possess Raman scattering features such as radial breathing mode (RBM) and tangential mode (G-band). These are sharp and strong peaks and are easily distinguished from fluorescence backgrounds.[23] The large aspect ratio and good integration with biomolecules further increases the SWCNT/AuNP nanohybrid's potential for applications.[21–25a,b] Ray and co-workers have reported SERS studies of SWCNT by attachment of gold nanoparticles on oxidized SWCNTs.[25a,b] They oxidized the SWCNTs by treatment with a mixture of strong concentrated acids and thionyl chloride, that exhibited good reactivity toward aminothiols.[25a,b] However, this treatment tends to generate new defect sites along the walls of SWCNTs. Strong oxidants have been reported to etch/destroy the graphene-like structure of the SWCNTs[26,27] and drastically decrease Raman signals of SWCNTs by many orders of magnitude.[23] Similarly, an issue that needs further attention is the less impressive aqueous stability and the low reproducibility of the SERS response from the different sites on SERS-based gold decorated SWCNT substrates. This is caused by the random aggregation of the SWCNT due to the strong van der Waal's forces and non-uniform attachment of noble metal particles on the SWCNTs surface due to the non-optimal functionalization strategies of SWCNTs and their poor dispersion during AuNP attachment. Hence the fabrication of SERS substrates with optimized properties is an on-going investigation that has attracted the interest of many researchers.[21–25, 28–33]Recently, we have demonstrated that Rh6G-labelled spherical gold nanoparticles attached-SWCNTs provide SERS spectra for indirect detection of bacteria suspended in water.[28]

NIH-PA Author Manuscript

NIH-PA Author Manuscript

NIH-PA Author Manuscript

Bacteria strains that are resistant to antibiotics are on the rise. Specifically, the outer membrane in gram-negative bacteria provides an additional layer of protection that contributes to bacteria resistance against antibacterial agents such as antibiotics, biocides, etc. Recently, gold nanoparticles have attracted a lot of attention as novel light-induced heating agents. Their heating efficiencies can be tailored by controlling their size and shape. [34] Light-induced heating by SWCNTs have also gained much attention lately. SWCNTs have good photothermal properties with excellent absorption in the NIR.

In this study, we hypothesized that multifunctional label-free AuNP@SWCNT hybrid nanomaterial probes with good SERS sensitivity and better photothermal properties can be achieved by controlling both electronic and chemical effects of the hybrid substrate. To improve sensitivity, we have used ~ 35 nm popcorn-shaped gold nanostructures for electromagnetic enhancement of SERS signals. The presence of sharp edges or tips on metal nanoparticles has been shown to increase electric-field enhancement which is important for applications involving metal nanoparticles as sensors.[35] For chemical enhancements, we have used the Raman active molecules (4ATP and the phenyl rings) covalently bonded to SWCNTs. Chemical bonding and the local symmetry of the benzene rings have been identified as the factors that contribute to Raman enhancement.[36] To improve stability and photothermal properties, the f_3-SWCNTs are selected as useful templates to generate uniform attachment of the gold nanopopcorns. Selectivity has been integrated through the use of target-specific recognition monoclonal antibodies.

Nitrile imines are reactive 1,3-dipoles with moderate activation energy barriers and hence can facilely undergo 1,3-cycloaddition on the sidewall of single-walled carbon nanotubes. 1,3-dipoles have been widely studied for their reactivity with SWCNT surface by both experimental and theoretical researchers.[37–39]

In this paper, we describe the strategy to fabricate label-free, stable SERS substrate based on MW-promoted 1,3-cycloadditon reaction on pre-modified SWCNTs (f_1-SWCNTs), amide bond formation and subsequent uniform attachment of AuNPs on the modified SWCNTs to yield multi-functional AuNP@f_3-SWCNT substrates for detection and photothermal killing of bacteria (Scheme 1). The detailed synthetic procedures and substrate characterization are discussed below.

2 Experimental

2.1 Materials and Chemicals

SWCNTs (diameter 0.7–1.1nm and length 300–2300nm), triethylamine (Et_3N), hydrogen tetrachloroaurate trihydrate ($HAuCl_4 \cdot 3H_2O$), $NaBH_4$, trisodium citrate (TSC), silver nitrate, ascorbic acid, 4-Aminothiophenol (4-ATP) and cetyl trimethylammonium bromide (CTAB) were purchased from Sigma-Aldrich. The heterofunctionalized polyethylene glycol, Thiol-PEG-NHS (MW 3400) was purchased from Nanocs Inc. New York (U.S.A). *E. coli* antibody mAb13622 was purchased from the American Type Culture Collection (ATCC, Rockville, MD). *E. coli 49979* and *Salmonella DT104* bacteria were kindly donated by Dr. Hwang, Environmental Science Department- Jackson State University. The aromatic hydrazonoyl chloride used was prepared using protocol previously reported by us.[40]

NIH-PA Author Manuscript

NIH-PA Author Manuscript

NIH-PA Author Manuscript

2.2 Methods

(a) Oxidation of SWCNTs—30 mg SWCNTs were first modified under mild acid oxidation conditions by sonication for 15 mins and refluxing in 2.5 M nitric acid for 1 hr. This was vacuum filtered using PTFE membrane (0.2 μm), washed several times to neutral pH and dried under vacuum for 12 hrs at 50 °C.[41]

(b) Ester-modified SWCNTs (f_1-SWCNTs)—The dried acid modified SWCNTs were refluxed in thionyl chloride in the presence of a catalytic amount of DMF for 1 hr. Next, to the room temperature flask, n-butanol was slowly added and gradually heated to reflux at 70 °C for the next 1 hr. This mixture was cooled and filtered, re-dispersed in ethanol and filtered thrice through a PTFE membrane (0.2 μm) and dried under vacuum at 50 °C for 12 hrs.

(c) MW-promoted 1,3-cycloaddition of nitrile imine on SWCNTs (f_2-SWCNT)—The ester-modified SWCNTs (f_1-SWCNTs) were dispersed in 15 mL anhydrous chloroform ($CHCl_3$) in an ultrasonic bath under nitrogen atmosphere for 5 minutes. 0.4 mmol of the aromatic hydrazonoyl chloride in 2.5 mL dry $CHCl_3$ was added to the suspension of f_1-SWCNT and stirred for 1 minute. Next, 0.2 mmol triethylamine was added. The mixture was microwave-irradiated (MWI) at 105 °C under nitrogen atmosphere for 30 mins (S1[†]). The above additions were repeated after 30 mins and irradiation was continued for the next 30 minutes under the same conditions to form the doubly ester-terminated SWCNTs cycloadduct (f_2-SWCNTs). The cooled reaction mixture was filtered through a PTFE membrane (0.2 μm), and washed with $CHCl_3$ and ethanol and left to dry overnight under a vacuum at 50 °C.

(d) MW-promoted amide bond formation (f_3-SWCNTs)—Next, doubly ester-terminated pyrazoline-modified SWCNTs were dispersed in 15 mL aqueous ethanol in an ultrasonic bath under 1min. A solution of 4-ATP in 3 mL aqueous ethanol was added and the mixture was MWI at 130 °C and 5 bars for 1 hr. The cooled reaction mixture was filtered through a PTFE membrane (0.2 μm), washed with aqueous ethanol and nanopure water.

(e) Preparation and attachment of gold nanopopcorns (AuNPs) to f_3-SWCNTs (AuNP@f_3-SWCNTs)—Gold nanopopcorns were prepared via a slightly modified two-step process reported by Ray and co-workers.[25].

i) Seed preparation: Briefly, the seed solution was prepared by mixing 20.0 mL nanopure water with 0.5 mL 0.01 M $HAuCl_4$ and 0.2 mL 0.025 M TSC. Freshly prepared ice-cold (ca. 0 °C) $NaBH_4$ (10 mM, 0.06 mL) was added with vigorous stirring. The solution turned pink immediately after the addition of $NaBH_4$. It was kept in the dark for 2–3 hours before use during which it turned red. This seed solution was used for the synthesis of gold nanopopcorns.

[†]Electronic Supplementary Information (ESI) available: [Additional Experimental details, figures showing attachment of gold nanopopcorns onto SWCNTs using different approaches, tables of hybrid nanomaterial concentration- and time- dependent microorganism viability studies, and viability rate of *Salmonella DT104* and *E. coli* upon 15 mins of 670 nm, 1.5–2.5Wcm-2 laser exposure under different conditions, TEM of *Salmonella DT 104* in presence of mAb-AuNP@f_3-SWCNT, Linearity of detection]. See DOI: 10.1039/b000000x/

NIH-PA Author Manuscript

NIH-PA Author Manuscript

NIH-PA Author Manuscript

ii) Gold nanopopcorns: 0.49 g of CTAB was dissolved in 45 mL H_2O in a 50 mL beaker, and 2 mL of 0.01M $HAuCl_4 \cdot 3H_2O$ was added under constant stirring. 0.3 mL of 0.01 M $AgNO_3$ was then added to the solution to mix properly. 0.32 mL of 0.1 M ascorbic acid was added dropwise as the weak reducing agent. The solution turned colourless. To this colourless solution was instantly added 0.5 mL of gold seed at a time and stirred for 1 min. The solution colour changed to blue within 2 minutes indicating the formation of popcorn-shaped gold nanostructures. The solution was kept at room temperature for 12 hours and centrifuged at 4800 rpm for 1½ hours to get rid of excess CTAB and any other unbound substrates.

(f) Antibody conjugation with AuNP@f_3-SWCNTs—The AuNP@f_3-SWCNTs were separated from water via centrifugation at 3500 rpm for 45 minutes, and washed twice with anhydrous ethanol. In order to conjugate the mAb onto the AuNP, the sulfhydryl and NHS heterofunctionalized polyethylene glycol (HS-PEG-NHS) linker were first anchored to the surface of the AuNPs. 50 μL (5 mM) of the HS-PEG-NHS linker was added to 2 mL of AuNP@f_3-SWCNTs in anhydrous ethanol, and the resulting mixture was allowed to react for 6 h at 4 °C in order to form stable thiol monolayers on the AuNPs. The mixture was next centrifuged at 3500 rpm for 20 min, washed with anhydrous ethanol to remove excess unanchored linker and re-dispersed in 2 mL PBS. For conjugation of mAb, 20 μL (0.1 mg/mL) of mAb was added to the NHS ester activated hybrid nanostructure. The solution was slowly mixed for 5 min at room temperature, and allowed to further react at 4 °C for 12 h. The NHS group reacts with the antibody's amine groups rapidly and allowed the antibody to immobilize onto the AuNP@f_3-SWCNTs. To remove any unbound antibodies and by-products, the resulting bioconjugated hybrid nanostructure (mAb-AuNP@f_3-SWCNT) suspension was centrifuged at 2500 rpm for 15 min; the precipitate was washed twice with PBS buffer and re-dispersed in 2 mL PBS buffer. This was stored at 4 °C for further use.

(g) Preparation of bacterial samples and SERS measurements

Before each microbiological experiment, all samples and glassware were sterilized by autoclaving at 121 °C for 15 mins at high pressure (0.1 MPa): *E. coli (49979)* and *Salmonella DT104* were cultivated in Luria broth (LB) and Tryptic Broth (TB) respectively at 37 °C with shaking at 220 rpm for 12 hrs. From the growth culture, a loop of bacteria was streaked on Luria agar (LA) plate and Tryptic agar (TA) plate respectively and incubated for 18 hrs at 37 °C. A single colony from LA/TA plate was inoculated into LB/TB (10 mL) and incubated at 37 °C with shaking at 220 rpm for 16 hrs. The bacterial sample was centrifuged at 3000 rpm for 10 minutes. The supernatant was discarded, and the bacterial sample was washed twice with 0.9% saline solution to yield a final bacterial concentration of approximately 1.3×10^8 CFU/mL. We performed serial dilutions of the bacteria to vary the concentration of bacteria samples from 1.3×10^8 to 10^1 CFU/mL. This solution was used as the working bacterial dilution. Typically, the mAb-AuNP@f_3-SWCNTs (50 μL) were added to 300 μL of solution containing ~10^1—10^8 colony forming units (CFU)/mL of *E. coli* , suspended in sterilized physiological saline solution with 0.5% BSA. The mixture were incubated in an orbital shaking incubator (OSI500R, TKS) operated at 120 rpm and 25 °C for 30 min. The sample was washed three times with sterilized physiological saline solution

NIH-PA Author Manuscript

NIH-PA Author Manuscript

NIH-PA Author Manuscript

before the Raman performance and TEM imaging (S1 †). All the reported concentrations are before mixing with the nanomaterial.

2.3 Characterization techniques and Raman measurements

The samples were examined using Transmission electron microscope (TEM) JEM-2100F (JEOL, Tokyo Japan) at 200 kV .UV/Vis absorption spectra were obtained using UV-Shimadzu 2600/2700 UV/Vis/NIR spectrophotometer, which is run by Varian's Cary Win UV software version 2.0. FTIR spectra of f_3-SWCNT were acquired using a Nexus 670 FTIR (Thermo Nicolet, Madison, WI) equipped with a universal attenuated total reflection (UATR) accessory, detector, and a KBr beam splitter. All spectra were averaged over 128 scans at a resolution of 4 cm^{-1}. Peak information was obtained using OMNIC software provided by Thermo Nicolet. For the SERS experiment, we used a continuous wavelength diode-pumped solid-state (DPSS) laser operating at 670 nm as an excitation light source with a power output of 2 mW on the sample. For excitation and data collection, we used InPhotonics 670 nm Raman fiber optic probe, which is a combination of two single fiber-optic cables, (90 micron excitation, 200 micron collection fiber) with filtering and steering micro-optics; N.A. 0.22. For Raman signal collection, we used a miniaturized QE65000 Scientific-grade Spectrometer from Ocean Optics, with a response range of 220–3600 cm^{-1}. The Hamamatsu FFT-CCD detector used in the QE65000 provides 90% quantum efficiency, with high signal-to-noise and rapid signal processing speed as well as remarkable sensitivity for low-light level applications. The Raman spectrum was analyzed with Ocean Optics data acquisition Spectra Suite spectroscopy software. We have used 20 s acquisition time and 5 scan averaging. SERS data was collected from three different areas on each sample at room temperature.

3 Results and discussion

3.1 Synthesis of AuNP@f_3-SWCNT hybrid nanomaterial

The attachment of the AuNP layer on individual SWCNTs was achieved through a four-step synthetic approach, as illustrated in Scheme 1. The Carboxyl groups on the SWCNTs were introduced via mild acid oxidation conditions that targeted only the initial defects that already existed on the SWCNTs.[26, 27] These were subsequently reacted with thionyl chloride and n-butanol to form the ester-modified SWCNT (f_1-SWCNT) which was used as the precursor for the pyrazoline/nitrile imine functionalized SWCNTs during the 1,3-cycloaddition reaction under MW irradiation[39, 42–43] (Scheme 1). The electron withdrawing ester groups activate the double bonds in the SWCNT graphitic structure enabling a facile 1,3-cycloaddition reaction with the *in-situ* generated nitrile imine dipoles under MW conditions in 1hr. Besides, the ester groups improved the hydrophilicity and stability of the f_2-SWCNT in aqueous media. Attempts to carry out 1,3-cycloaddition, or acid-modification reactions with pristine SWCNTs under similar conditions yielded modified SWCNTs with less dispersion in aqueous media (Figure S2-A,B,C†). The highly ester-terminated pyrazoline-grafted SWCNTs underwent further amide bond formation upon reaction with 4-ATP under microwave conditions[44–46] in under 1hr to yield the highly SH-terminated f_3-SWCNTs (Scheme 1). No obvious aggregation of nanotubes was noticed during this step. The f_3-SWCNTs were characterized by FTIR, TEM and UV-Vis. The Fourier transform

NIH-PA Author Manuscript

NIH-PA Author Manuscript

NIH-PA Author Manuscript

infrared (FT-IR) spectrum of f_3-SWCNT (Figure 1) show the overlapping C-N stretch and aromatic in-plane C-H bending at 1200-1030 cm^{-1}. Intense C=N stretch (1620-1550 cm^{-1}) centered around 1590 cm^{-1} and aromatic C=C stretch at 1620 cm^{-1} that are presumed to arise from the bonds formed during the 1,3-cycloaddition reaction between the SWCNTs and the *in-situ* generated nitrile imine can also be seen. Amide carbonyl peak -C=O at ~1650 cm^{-1}, and the secondary amide –N-H stretch at ~3340 cm^{-1} can also be seen in the spectra.

This FTIR data confirms the successful amide bond formation. Other peaks due to C–C stretch (in-ring) at 1400 cm^{-1} and a weak –SH stretch at 2600 cm^{-1} were also visible. The -SH terminals were used to attach AuNPs through the well-known Au-S bond (Scheme 1 and S1†).

Transmission electron microscopy (TEM) images (Figure 2A) illustrate the morphology of the AuNPs used. The AuNPs averaged 35 nm in size and had multiple sharp tips and edges, with small central spherical regions acting as electron reservoirs and a maximum absorbance at 570 nm.

Gold nanoparticles of sizes greater than 20 nm, with sharp tip and edge have been reported capable of enhancing Raman signals via the well-studied "lightning-rod effect".[18, 47–48] Figure 2B shows the TEM image of f_3-SWCNT dispersions. Figure 2C shows the TEM image illustrating the morphology of AuNP@f_3-SWCNT hybrid nanostructure. Few exposed parts of nanotubes were observed (Figure 2C), indicating a near complete AuNPs layer on the SWCNT surface, an evidence for the presence of an abundant supply of SH-terminated functional groups on the nanotube walls. AuNPs attached along f_3-SWCNTs in a pseudo-1-D morphology, with very minimal level of aggregation and at a minimum inter-particle distance. This implied an efficient functionalization of the SWCNTs and stable dispersions of the f_3-SWCNTs. The uniform dense attachment of the AuNPs on the f_3-SWCNTs result in effective plasmon coupling that has been reported to cause signal enhancement via "hot-spot phenomenon."[49] Upon attachment of the AuNPs to the f_3-SWCNTs, the absorbance red-shifts and broadens out implying successful attachment of the AuNPs (Figure 2D-blue). The UV-Vis-NIR spectrum of f_3-SWCNTs (Figure 2 D-red) was largely featureless and free of Van Hove singularities, a characteristic associated with successful modification of SWCNTs.

3.2 SERS studies of AuNP@f_3-SWCNT hybrid nanomaterial

The SERS spectra of our AuNP@f_3-SWCNT were investigated by using a 670 nm laser excitation source. We observed changes in the relative intensities and shifts in the peak frequencies of several vibrational modes of the f_3-SWCNTs upon attachment of AuNPs that indicate specific interactions between the f_3-SWCNTs and the AuNP nanostructure surface. Figure 3 shows the comparison of the Raman spectra of f_3-SWCNT and AuNP@f_3-SWCNT (Fig. 3A), and AuNP@f_3-SWCNT and concentrated acid mixture modified AuNP@SWCNTs (Fig. 3C). The characteristic peak, namely the G-band peak at ~1600 cm^{-1} can be seen in all of the spectra. The low intensity D- band peaks at ~1350 cm^{-1} in the spectra of f_3-SWCNT and AuNP@f_3-SWCNT was ascribed to modification at the original defect sites of the SWCNTs. The less intense D-bands can be interpreted to imply negligible extra defects created on the SWCNTs and therefore conservation of the quality of the

NIH-PA Author Manuscript

NIH-PA Author Manuscript

NIH-PA Author Manuscript

SWCNTs. In Figure 3A, the new bands at 480 cm^{-1} δ(CS), ~1080 cm^{-1} ν(CS), 1145 cm^{-1} δ(CH) and 1390 cm^{-1} ν(CC) + δ(CH), are due to chemical modification.[50–51] These bands are absent in the Raman spectrum of pristine SWCNTs, (Figure. 3(B) (a)). To help interpret the spectra in Figure 3(A), the Raman spectrum of 4-ATP adsorbed on AuNPs (Figure 3(B) (b)) was acquired. The Raman spectrum of 4-ATP has bands at 464 cm^{-1} δ(CS), 890 cm^{-1} associated with π(CH) + δ(SH), 1089 cm^{-1} ν(CS), 1439 cm^{-1} ν(CC) + δ(CH) and 1595 cm^{-1} ν(CC). [50–51] Hence the observed bands in Figure 3A can be interpreted to originate with the numerous phenyl rings used as starting materials during the modification. The shifts in the peak frequencies in Figures 3(A) and (B) (b) provide evidence for significant chemical bonding. The chemical shift of peak at ~1440 cm^{-1} and overlap of the peak at 1595 cm^{-1} with the G-band results in a much stronger peak at ~1600 cm^{-1}. Figure 3(C) shows a comparative D-band study between AuNP-attached SWCNTs modified via concentrated strong acid mixture route and our strategy. Substantial D-band defects exist in 3(C) (a). Hence our modification strategy significantly enhanced the peak at ~1600 cm^{-1}, resulted in more characteristics Raman signature peaks and conserved quality of the SWCNTs in accordance with our hypothesis and other similar studies.[52, 53]

Beside the additional enhancement of the Raman signal at 1600 cm^{-1}, the spectral profiles for AuNP@f_3-SWCNTs and f_3-SWCNT are very similar which indicate specific interactions of the f_3-SWCNTs with the AuNPs surface.

The observed enhancement in the SERS signal of the AuNP@f_3-SWCNT is proposed to result from: (i) an “electromagnetic” surface-enhanced Raman spectral (SERS) enhancement due to resonances between the energy of the excitation laser and the electronic excitations in the roughened AuNPs nanostructures, the strong field coupling effects due to the close proximity of sharp tip and edge AuNP attached along the SWCNTs and (ii) a “chemical” SERS enhancement due to the interactions between the f_3-SWCNTs’ and the AuNPs surfaces, and a “selective resonance Raman effect” at wavelength of ~1600 cm^{-1} due to overlap/chemical shifts of peaks during the functionalization of the SWCNT (f_3-SWCNTs).

3.3 Antibody conjugation

HS-PEG-NHS (MW 3400) ester was next used to further stabilize the hybrid nanomaterial, block the surface of AuNPs to prevent incidences of non-specific binding and provide the reactive terminal for antibody conjugation (Figure 4). The antibody conjugated NHS-PEG-AuNP@f_3-SWCNT was found to be stable in PBS solution. The UV-Vis-NIR spectra for antibody conjugated NHS-PEG-AuNP@f_3-SWCNT showed no significant change 3 weeks later. The stability was further confirmed by the TEM images that showed no significant differences from the ones taken 3 weeks earlier (Figure S2-D[†]). This demonstrates the high stability of the hybrid nanostructure.

3.4 Bacterial capturing selectivity

The bacterial binding affinity of mAb-AuNP@f_3-SWCNTs was tested against both *E. coli 49979* and *Salmonella DT104* bacterial strains and evaluated on the basis of selectivity and sensitivity by UV-Vis, OD measurements, TEM and Raman spectroscopy. The AuNP@f_3-SWCNTs hybrids nanomaterial was conjugated to monoclonal *E. coli* antibody (*mAb 13622*)

NIH-PA Author Manuscript

NIH-PA Author Manuscript

NIH-PA Author Manuscript

through the SH-PEG-NHS (MW 3400) ester linker as illustrated in Figure 4. Figure 5A shows the UV-Vis absorbance spectra of unconjugated monoclonal *E. coli* antibody, (blue), activated AuNP@f_3-SWCNTs (black) and, mAb-AuNP@f_3-SWCNTs hybrid nanomaterial after conjugation with the antibody (red).

The additional absorption peak at ~280 nm on the spectrum (red curve) demonstrated that the antibody had been successfully conjugated to the hybrid nanomaterial. To investigate the bacteria capturing selectivity of the mAb-AuNP@f_3-SWCNT, we incubated 1.3×10^8 CFU/mL of *E. coli*, and *Salmonella DT104* with the mAb-AuNP@f_3-SWCNTs and studied the absorption profile of the suspensions at OD_{600} at room temperature for 16 minutes (see S1†). The optical density at 600 nm (OD_{600}) was used to infer the density of bacteria in the medium.[54] The absorption profile, Figure 5(B), shows that the OD_{600} drastically decreased when *E. coli* was incubated with mAb-AuNP@f_3-SWCNT nanomaterial (blue bars) but insignificantly decreased for *Salmonella* bacterial strains (green bars), implying that our antibody conjugated-AuNP@f_3-SWCNT possessed bacteria capturing selectivity towards *E. coli* but not *Salmonella DT104* bacterial strain. The *Salmonella* bacterial concentration in suspension remained high while that of *E. coli* significantly decreased due to *E. coli* immobilization by the antibody-conjugated hybrid nanomaterial. The OD_{600} for the hybrid nanomaterial suspension with *E. coli* decreased from 0.955 to 0.843, whereas in the case of *Salmonella*, OD_{600} decreased from 0.923 to 0.870 only in 15 minutes.

3.5 Bacterial detection and quantification

Bacterial detection and quantification is demonstrated in Figure 6(A)–(D). The TEM images show *E. coli* bacteria closely bound to the mAb-conjugated hybrid nanostructure (Figure 6A) forming clusters of *E. coli*, but not *Salmonella DT104* (Figure S4†). The close binding of *E. coli* is mediated by the *E. coli* monoclonal antibody conjugated on the hybrid nanostructure. The typical rod-like shape of *E. coli* is distorted unlike *Salmonella DT104* (Figure S4†). This may be due to binding selectivity that may elicit the unexpected morphological changes in *E. coli* so as to facilitate their adaptation in the new environment. Fig. 6(B) shows the average of 3 SERS readouts taken from different positions of *E. coli* immobilized on the mAb-AuNP@f_3-SWCNTs at different concentrations of *E. coli* (10^8-10^1 CFU/mL). The *E. coli* immobilized onto the mAb-AuNP@f_3-SWCNTs SERS-active probe formed microbial clusters that resulted in significant SERS enhancement. The spectra are consistent in shape with significant variations in the intensity of the key peak at ~1600 cm^{-1} that was proportional to the concentration of the *E. coli*. This implied good spectral reproducibility from our SERS-active hybrid probe which was important for biological sample measurements.

The use of functionalized SWCNTs (f_3-SWCNTs) helped overcome challenges associated with reproducibility and signal stability. The relative intensity of the SERS signals from the hybrid nanomaterial peaks increased with increasing concentration of *E. coli* up to 10^6 CFU/ml. The G-band at ~1600 cm^{-1} was chosen for quantitative analysis based on its intensity dependence on *E. coli* concentrations. Figure 6C shows high resolution SERS response for the increased intensity of the 1600 cm^{-1} G-band with the increase of *E. coli* concentrations. At *E. coli* concentrations $10^2 \leq X \geq 10^6$ CFU/mL, the peak intensity of the G-

NIH-PA Author Manuscript

NIH-PA Author Manuscript

NIH-PA Author Manuscript

band increased with increase in concentration of *E. coli*. Further increase in concentration to 10^7 CFU/mL or higher, resulted in a drop in intensity. The detection sensitivity of our mAb-AuNP@f_3-SWCNT hybrid for *E. coli* was 10^2 CFU/mL and had a linear detection range between 10^2 and 10^6 CFU/mL (Figure 6D and Figure S5†). The impressive linear range can be used to quantify the number of microorganisms in per unit volume of a sample. The sensitivity of *E. coli* detection was associated with the efficiency of functionalization of SWCNTs and the subsequent attachment of the sharp tip and edge plasmonic AuNPs. The greater the functionalization, the more attached the AuNPs and an increase in more conjugated antibodies gives rise to a more responsive hybrid nanomaterial. To verify that the SERS signal change of the G-band was specific to recognition of *E. coli*, we tested our mAb-AuNP@f_3-SWCNT hybrid with *Salmonella DT104*. The SERS response of the hybrid nanomaterial at equal concentrations of *E. coli* and *Salmonella DT104* (10^5 CFU/mL) showed a much lower intensity change in response to *Salmonella DT104* but a much greater intensity change for *E. coli* at the same CFU/mL. This further confirmed that our antibody conjugated-AuNP@f_3-SWCNT possessed bacteria capturing selectivity towards *E. coli* but not the *Salmonella DT104* bacterial strain.

3.6 Cytotoxicity and Antibacterial Photothermal Studies

In order to determine the cytotoxicity of the hybrid nanomaterial toward *E. coli*, 1.3×10^3 CFU/mL (10^{-5} dilutions) of *E. coli* were immobilized on different amounts of mAb-AuNP@f_3-SWCNT and incubated on agar plates at 37 °C for 18 hrs. *E. coli* incubated in the absence of the nanomaterial was used as the control. Our results show over 94% bacterial viability in a 1:1 (hybrid: cells) ratio (Table S3-a†). Next, 1.3×10^3 CFU/mL of *E. coli* were incubated with mAb-AuNP@f_3-SWCNT hybrid in the ratio 1:3 (hybrid: cells) for up to 10 hrs at room temperature. The treated samples incubated at increasing hour increments were plated on agar and incubated at 37 °C for 18 hrs. Samples incubated with AuNPs were used as the positive controls. As shown in Figure 7A, *E. coli* viability of 94±3% was observed for hybrid nanomaterial (blue bars) with samples plated 10 hours after the incubation. This compares well with the reported values for samples that were incubated in AuNPs (red curves) and confirmed the non-toxicity of the nanomaterial.

To evaluate the antibacterial photothermal capabilities of our hybrid nanomaterial, we performed NIR laser exposure experiments using a protocol previously reported by us with slight modifications.[55] When both *E. coli* and *Salmonella* bacteria were exposed to the red light (670 nm OEM laser at 1.5–2.5 Wcm^{-2}) for 15 mins, the bacteria survival rate in the absence of hybrid nanomaterial was above 96% (Figure 7B,(II) and Table S3-b†), while in the presence of mAb-AuNP, *E. coli* viability was 59% (Figure 7B,(III)) as determined by colony count technique. In contrast, *E. coli* bacteria survival dramatically decreased upon NIR laser exposure in the presence of hybrid nanomaterial to 2.67±0.58% (Figure 7B and C (IV)). This shows that NIR laser exposure alone was harmless to the bacteria. The antibacterial photothermal activity of the hybrid nanomaterial was much better than that of the AuNPs alone.

Figure 7C, shows digital photographs and the number of colonies after 15 mins exposure to 670 nm light for *E. coli* (II), *E. coli* bound mAb-AuNPs (III) and *E. coli* bound mAb-

NIH-PA Author Manuscript

NIH-PA Author Manuscript

NIH-PA Author Manuscript

AuNP@f_3-SWCNT hybrid. At a higher concentration of *E. coli* (10^5CFU/mL), the viability of the treated bacterial cells was reduced by ≥90% after 15 minutes of exposure. This demonstrates the greater heating efficiencies of the AuNP@f_3-SWCNT hybrid nanostructures. Several groups have demonstrated photothermal bactericidal activities by using multi-branched gold nanoparticles[56–58] and single-walled carbon nanotubes.[25b] The hybrid nanostructures showed improved photothermal bactericidal activity in 15 mins.

When the hybrid nanomaterial was excited with 670 nm light, strong absorption by both the gold nanopopcorns and the f_3-SWCNT occur which synergistically resulted in a rapid and greater localized heating effect. This local temperature increase produced sufficient heat for the killing of bacteria, which could therefore be the next avenue for exploration to target and destroy water-borne microbes. However, it is important to note here that due to the mismatch in wavelength of absorption with the incident laser source, the richness of the Raman signature peaks and photothermal properties of our hybrid nanostructure was not fully realized.

Next, to understand whether our mAb-AuNP@f_3-SWCNT hybrid antibacterial photothermal agent was highly selective, we performed the same experiment with *Salmonella DT104*. For this purpose, we incubated 1.3×10^3 CFU/mL of *Salmonella DT104* suspension with mAb-AuNP@f_3-SWCNT nanomaterial. After 30 mins of incubation at room temperature with gentle shaking, we exposed the sample to light (670 nm at 1.5–2.5 Wcm^{-2}) for 15 mins. We observed that almost 85% of the *salmonella DT104* bacteria were still viable after 15 mins of treatment. Thus, our result clearly shows that bioconjugation of the photothermal hybrid nanomaterial with bacteria was necessary in order to realize significant photothermolysis. As demonstrated earlier (Figure 5B), because the *mAb13622* antibody conjugated AuNP@f_3-SWCNT hybrid had poor selectivity for *Salmonella DT104*, the bacteria in the suspension do not have enough absorption at 670 nm. Hence, during photothermal destruction using 670 nm light, the effective temperature increase around bacteria was very little, which was insufficient to kill these pathogens.

4 Conclusions

In summary, MW irradiation accelerated 1,3-cycloaddition of nitrile imines on SWCNTs was achieved. The modified SWCNTs were used to attach AuNPs and exhibited good SERS responses. The fabricated hybrid nanomaterial was subsequently conjugated to the *E. coli* antibody for selective detection and quantification of *E. coli*. At 670 nm light excitation, we demonstrated that the antibody conjugated AuNP@f_3-SWCNT hybrid nanomaterial can achieve impressive *E. coli* sensitivity and selectivity with good rapidity (>1 hr). The hybrid nanomaterial has good linear detection responses at an *E. coli* concentration range between 10^2 and 10^6 CFU/mL and a detection limit of 10^2 CFU/mL. The strong electromagnetic and chemical effects attributable to the components of the hybrid nanostructure significantly increase SERS-active enhancements and hence enable detection and quantification of *E. coli* in water for environmental monitoring. We have also demonstrated the hybrid nanomaterial as a rapid (~15 mins) and effective (~97% killing efficiency) photothermal agent toward *E. coli* when compared with AuNPs under a laser exposure of 670 nm, 1.5–2.5 Wcm^{-2} power. The detection and photothermal killing approach developed in this study can potentially be

NIH-PA Author Manuscript

NIH-PA Author Manuscript

NIH-PA Author Manuscript

used to detect and photothermally kill other pathogenic microorganisms such as the drug resistant *Salmonella DT104* by only changing the pathogen-specific antibody since the basic principle of the SERS sensor remain the same.

Supplementary Material

Refer to Web version on PubMed Central for supplementary material.

Acknowledgments

The work described was supported by the National Science Foundation (HBCU-RISE: HRD-1137763, PREM: DMR-633156), the National Institutes of Health through the NCRR-RCMI (Award Number: G12RR13459), and NIH/NIMHD (Award Number: G12MD007581) for the use of the Analytical CORE Facilities.

References

1. Ciosek P, Wróblewski W. Sensors. 2011; 11:4688–4701. [PubMed: 22163870]
2. Wang S, Singh AK, Senapati D, Neely A, Yu H, Ray PC. Chem. A Eur. J. 2010; 16:5600–5606.
3. Rosi NL, Mirkin CA. Chem. Rev. 2005; 105:1547–1562. [PubMed: 15826019]
4. Perez FG, Mascini M, Tothill IE, Turner APF. Anal. Chem. 1998; 70:2380–2386. [PubMed: 9624909]
5. Klodzinska E, Dahm H, Rozycki H, Szeliga J, Jackowski M, Buszewski B. J. Sep. Sci. 2006; 29:1180–1187. [PubMed: 16830734]
6. Wu W, Zhang J, Zheng M, Zhong Y, Yang J, Zhao Y, Ye W, Wen J, Wang Q, Lu J. PLoS One. 2012; 11:e48999. [PubMed: 23145045]
7. Naja G, Bouvrette P, Hrapovic S, Luong JHT. Analyst. 2007; 132:679–686. [PubMed: 17592587]
8. Nie S, Emroy RS. Science. 1997; 275:1102–1106. [PubMed: 9027306]
9. Cao CY, Jin R, Mirkin CA. Science. 2002; 297:5586. 1536–1540.
10. Zavaleta CL, Smith BR, Walton I, Doering W, Davis G, Shojaei B, Natan MJ, Gambhir SS. Proc. Natl. Acad. Sci. U.S.A. 2009; 106:13511–13516. [PubMed: 19666578]
11. Patel IS, Premasiri WR, Moir DT, Ziegler LD. J. Raman Spectroscopy. 2008; 39:1660–1672.
12. Golightly RS, Doering WE, Michael JN. ACS Nano. 2009; 3:2859–2869. [PubMed: 19856975]
13. Chen LM, Li YN. ACS Appl. Mater. Interfaces. 2011; 3:3091–3096. [PubMed: 21744828]
14. Dasary SSR, Singh AK, Senapati D, Yu H, Ray PC. J. Am. Chem. Soc. 2009; 131:13806–13812. [PubMed: 19736926]
15. Premasiri WR, Moir DT, Klempner MS, Krieger N, Jones G, Ziegler LD. J. Phys. Chem. B. 2005; 109:312–320. [PubMed: 16851017]
16. Wang Y, Lee K, Irudayaraj J. J. Phys. Chem. C. 2010; 114:16122–16128.
17. Chae EJ, Lee JH, Oh BK, Choi JW. J Biomed Nanotechnology. 2013; 9:659–663.
18. Pazos-Pérez N, Barbosa S, Rodríguez-Lorenzo L, Aldeanueva-Potel P, Pérez-Juste J, Pastoriza-Santos I, Alvarez-Puebla AR, Liz-Marzán ML. J. Phys. Chem. Lett. 2010; 1:24–27.
19. Kahraman M, Yazici MM, Sahin F, Bayrak OF, Çulha M. Appl. Spectrosc. 2007; 61:479–485. [PubMed: 17555616]
20. Sengupta A, Laucks ML, Davis EJ. Appl. Spectrosc. 2005; 59:1016–1023. [PubMed: 16105210]
21. Sun Y, Liu K, Miao J, Wang Z, Tian B, Zhang L, Li Q, Fan S, Jiang K. Nano Lett. 2010; 10:1747–1753. [PubMed: 20387801]
22. Chu H, Wang J, Ding L, Yuan D, Zhang Y, Liu J, Li Y. J. Am. Chem. Soc. 2009; 131:14310–14316. [PubMed: 19764748]
23. Wang X, Wang C, Cheng L, Lee ST, Liu Z. J. Am. Chem. Soc. 2012; 134:7414–7422. [PubMed: 22486413]

NIH-PA Author Manuscript NIH-PA Author Manuscript NIH-PA Author Manuscript

24. Chen Z, Tabakman SM, Goodwin AP, Kattah MG, Daranciang D, Wang X, Zhang G, Li X, Liu Z, Utz P, Jiang K, Fan S, Dai H. Nat. Biotechnol. 2008; 26(11):1285–1292. [PubMed: 18953353]
25. (a) Beqa L, Singh AK, Fan Z, Senapati D, Ray PC. Chem. Phys. Lett. 2011; 512:4–6. 237–242. (b) Beqa L, Fan Z, Singh AK, Senapati D, Ray PC. ACS Appl. Mater Interfaces. 2011; 3:3316–3324. [PubMed: 21842867]
26. Zhang J, Zou H, Qing Q, Yang Y, Li Q, Liu Z, Guo X, Du Z. J. Phys. Chem. B. 2003; 107:3712–3718.
27. Tchoul MN, Ford WT, Lolli G, Resasco DE, Arepalli S. Chem. Mater. 2007; 19:5765–5772.
28. Lin Y, Hamme AT. Analyst. 2014; 139:3702–3705. [PubMed: 24897935]
29. Lee SJ, Guan Z, Xu H, Moskovits M. J. Phys. Chem. C. 2007; 111:17985–17988.
30. Han X, Wang H, Ou X, Zhang X. J. Mater. Chem. 2012; 22:14127–14132.
31. Ko H, Tsukruk VV. Small. 2008; 4:1980–1984. [PubMed: 18924130]
32. Qin L, Zou S, Xue C, Atkinson A, Schatz CG, Mirkin CA. Proc. Natl. Acad. Sci. U.S.A. 2006; 103(36):13300–13303. [PubMed: 16938832]
33. Fan M, Andrade SFG, Brolo GA. Anal. Chim. Acta. 2011; 693:7–25. [PubMed: 21504806]
34. Rodriguez-Oliveros R, Sanchez-Gil JA. Opt. Express. 2012; 20:621–626. [PubMed: 22274385]
35. Sánchez-Iglesias A, Pastoriza-Santos I, Pérez-Juste J, Rodríguez-González B, Javier García de Abajo F, Liz-Marzán LM. Adv. Mater. 2006; 18:2529–2534.
36. Saikin SK, Olivares-Amaya R, Rappoport D, Stopac M, Aspuru-Guzik A. Phys. Chem. Chem. Phys. 2009; 11:9401–9411. [PubMed: 19830323]
37. Yang T, Zhao X, Nagase S. J. Comput. Chem. 2013; 34:2223–2232. [PubMed: 23832655]
38. Lu X, Tian F, Xu X, Wang N, Zhang Q. J. Am. Chem. Soc. 2003; 125:10459–10464. [PubMed: 12926971]
39. Alvaro M, Atienzar P, De la Cruz P, Delgado JL, Garcia H, Langa F. J. Phys. Chem. B. 2004; 108:12691–12697.
40. Dadiboyena S, Hamme II AT. Tetrahedron Lett. 2011; 52:2536–2539. [PubMed: 21686095]
41. Wang Y, Iqbal Z, Malhotra SV. Chem. Phys. Lett. 2005; 402:96–101.
42. Langa F, de la Cruz P. Comb. Chem. High Throughput Screening. 2007; 10:766–782.
43. El-Kateb AA, Abd El-Rahman NM, Saleh, Ali TS, Hassan M, El-Dosoky AY, Ghada EAA. J. Appl. Sci. Res. 2012; 8:3393–3405.
44. Kakade BA, Pillai VK. Appl. Surf. Sci. 2008; 254:4936–4943.
45. Raghuveer MS, Agrawal S, Bishop N, Ramanath G. Chem. Mater. 2006; 18:1390–1393.
46. Liu R, Arrington MP, Hopper A, Tehim A. PCT/US. 2005/047439, WO 2006/071988.
47. Zhang W, Cui X, Martin OJF. J. Raman Spectrosc. 2009; 40:1338–1342.
48. Rodríguez-Lorenzo L, Alvarez-Puebla RA, Pastoriza-Santos I, Mazzucco S, Stéphan O, Kociak M, Liz-Marzaán LM, García de Abajo JF. J. Am. Chem. Soc. 2009; 131:4616–4618. [PubMed: 19292448]
49. Wei H, Xu H. Nano Scale. 2013; 5:10794–10805.
50. Kim K, Lee HS. J. Phys. Chem. B. 2005; 109:18929–18934. [PubMed: 16853437]
51. Kim K, Kim KL, Shin D, Choi JY, Shin KS. J. Phys. Chem. C. 2012; 116:4774–4779.
52. Kneipp K, Kneipp H, Dresselhaus MS, Lefrant S. Phil. Trans. R. Soc. Lond. A. 2004; 362:2361–2373.
53. Al-Attar N, Kopf I, Kennedy E, Flavin K, Giordani S, Rice JH. Chem. Phys. Lett. 2012; 535:146–151.
54. Nester, EW.; Anderson, DG.; Roberts, CE., Jr; Nester, MT. Microscopy and Cell Structure In Microbiology: A Human Perspective. Peterson, KA., editor. New York: McGraw-Hill; 2007. p. 55-82.
55. Fan Z, Senapati D, Khan SA, Singh AK, Hamme A, Yust B, Sardar D, Ray PC. Chem. Eur. J. 2013; 19:2839–2847. [PubMed: 23296491]
56. Ray PC, Khan SA, Singh AK, Senapati D, Fan Z. Chem. Soc. Rev. 2012; 41:3193–3209. [PubMed: 22331210]

57. Wang C, Irudayaraj J. Small. 2008; 4:2204–2208. [PubMed: 19003819]
58. Zharov VP, Mercer KE, Galitovskaya EN, Smeltzer MS. Biophys. J. 2006; 90:619–627. [PubMed: 16239330]

NIH-PA Author Manuscript
NIH-PA Author Manuscript
NIH-PA Author Manuscript

NIH-PA Author Manuscript
NIH-PA Author Manuscript
NIH-PA Author Manuscript

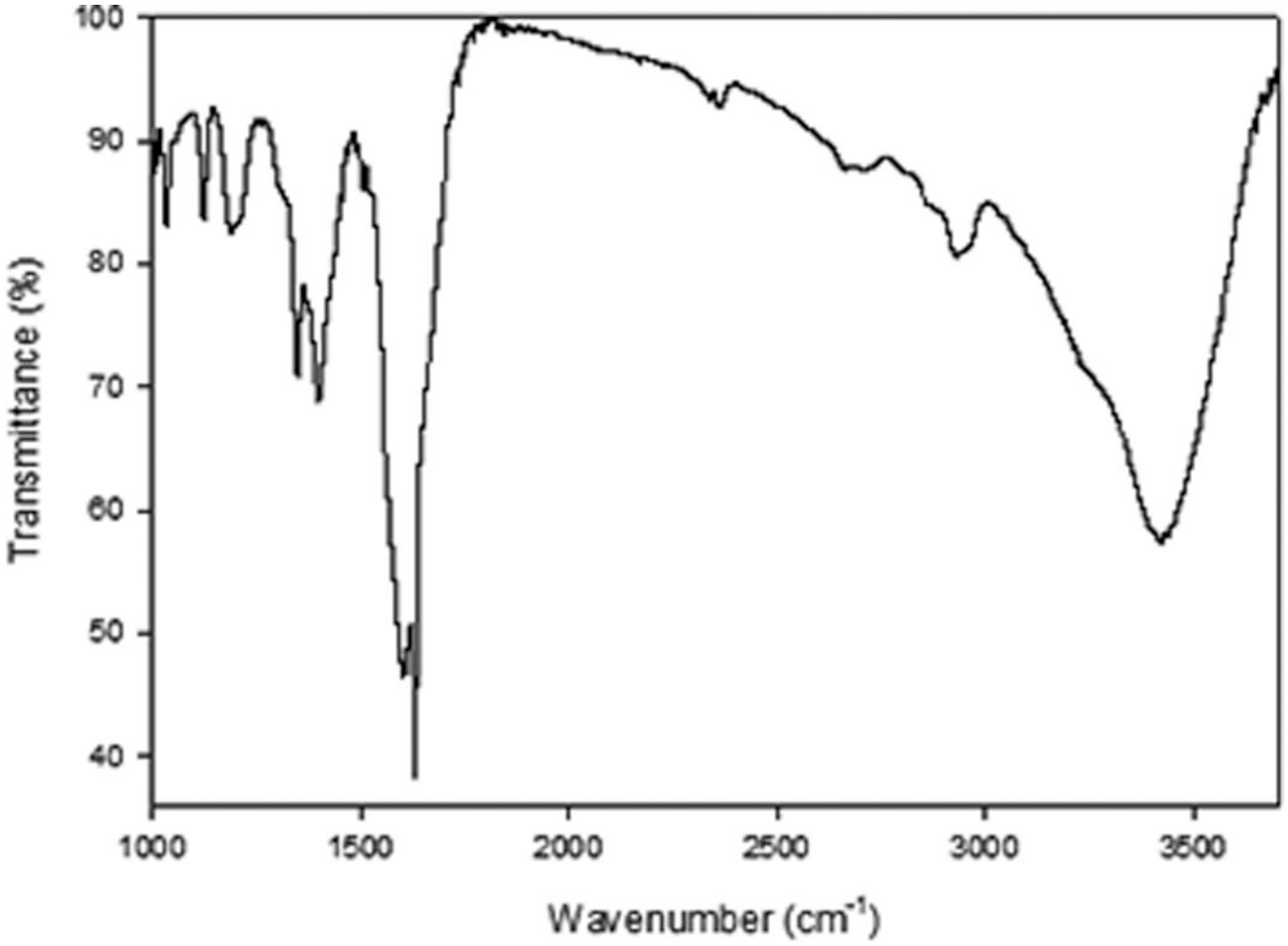

Figure 1.

FTIR spectra of modified SWCNTs (f_3-SWCNTs) that have undergone 1,3-cycloaddition and amide bond formation under MW promotion

NIH-PA Author Manuscript
NIH-PA Author Manuscript
NIH-PA Author Manuscript

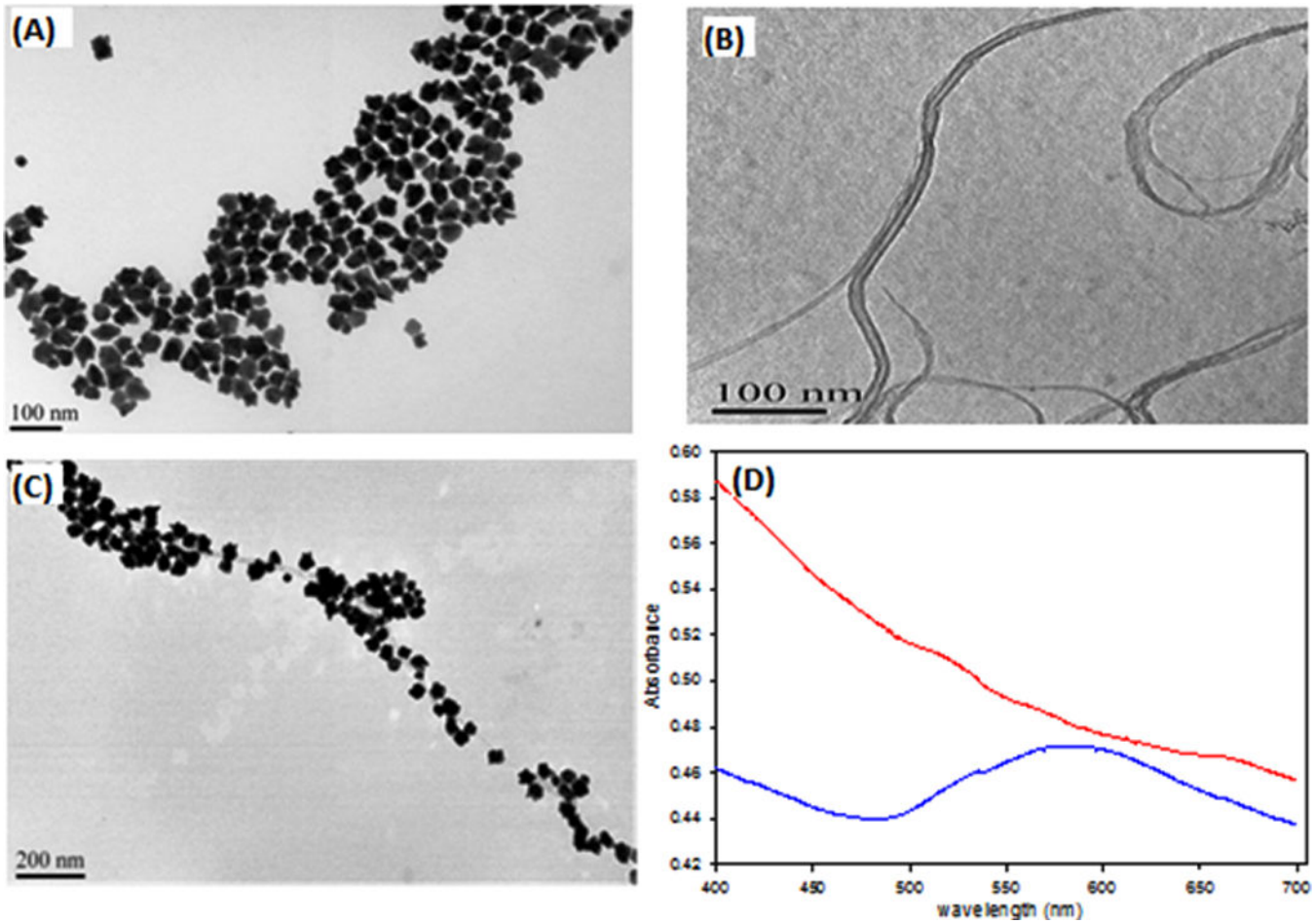

Figure 2.

Characterization of Gold nanopopcorns (AuNPs), f_3-SWCNTs and AuNP@f_3-SWCNT. (A) TEM image of AuNPs (B) TEM image of f_3-SWCNTs and (C) TEM image of AuNP@f_3-SWCNTs (D) UV-Vis spectra of f_3-SWCNTs (red) and AuNP@f_3-SWCNTs (blue)

NIH-PA Author Manuscript

NIH-PA Author Manuscript

NIH-PA Author Manuscript

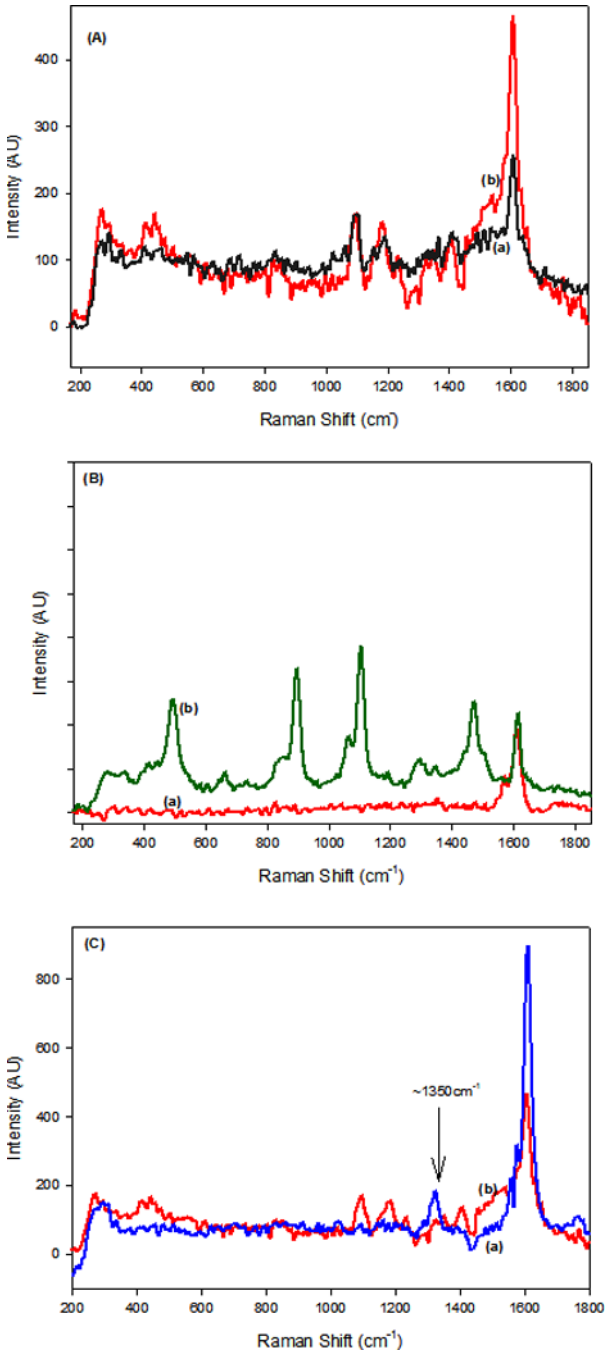

Figure 3.

Comparison of: (A) Normal Raman spectra of f_3-SWCNTs (a) and SERS spectra of AuNP@f_3-SWCNTs (b), (B) Raman spectra of pristine SWCNTs (a) and SERS spectra of 4-ATP adsorbed on AuNPs (b), (C) SERS spectra of AuNP attached- (a) concentrated acid modified SWCNTs and (b) f_3-SWCNTs

NIH-PA Author Manuscript

NIH-PA Author Manuscript

NIH-PA Author Manuscript

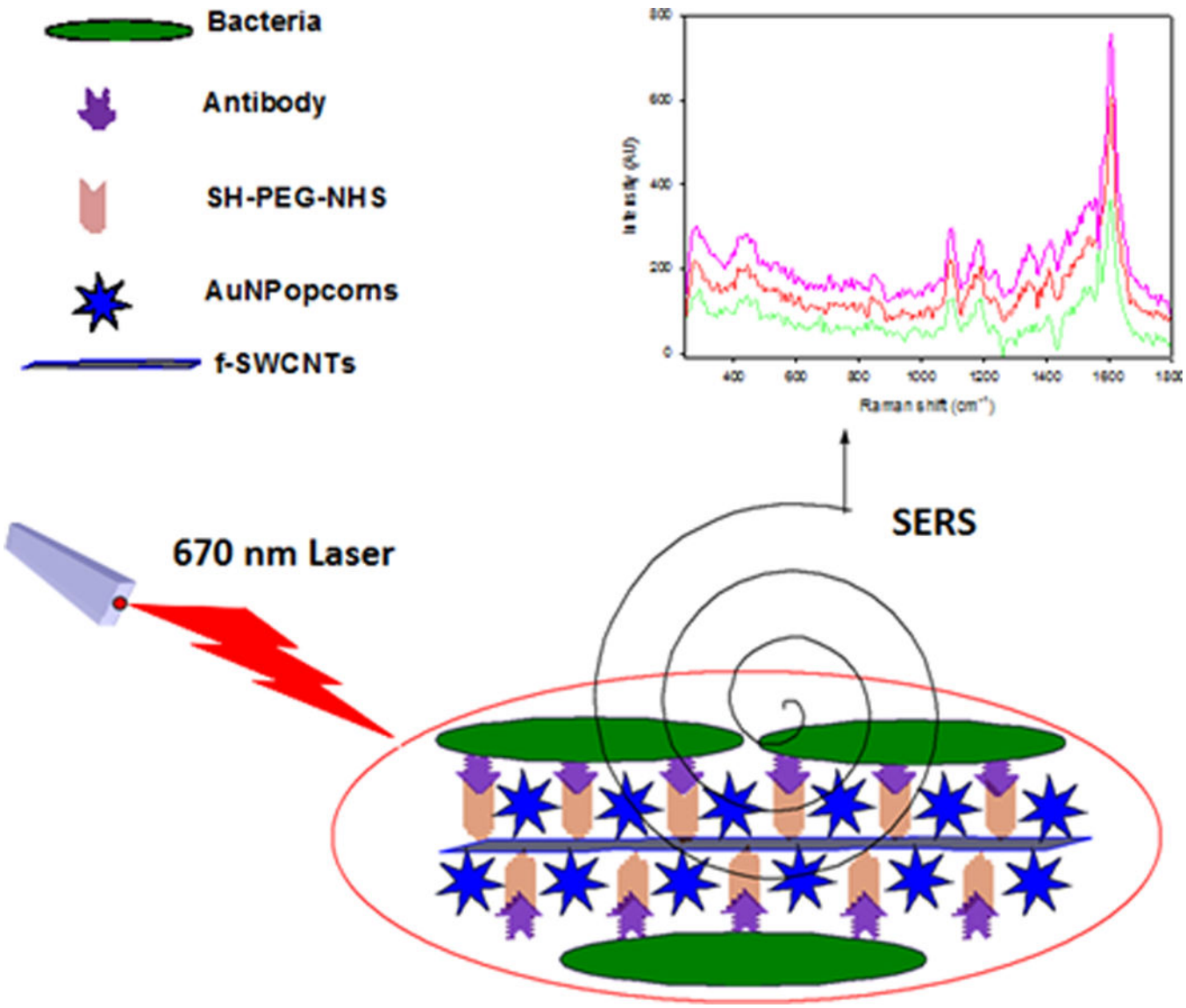

Figure 4.

Schematic illustration of the fabrication of antibody-conjugated AuNP@f_3-SWCNT SERS probe hybrid nanomaterial and detection of bacteria.

NIH-PA Author Manuscript

NIH-PA Author Manuscript

NIH-PA Author Manuscript

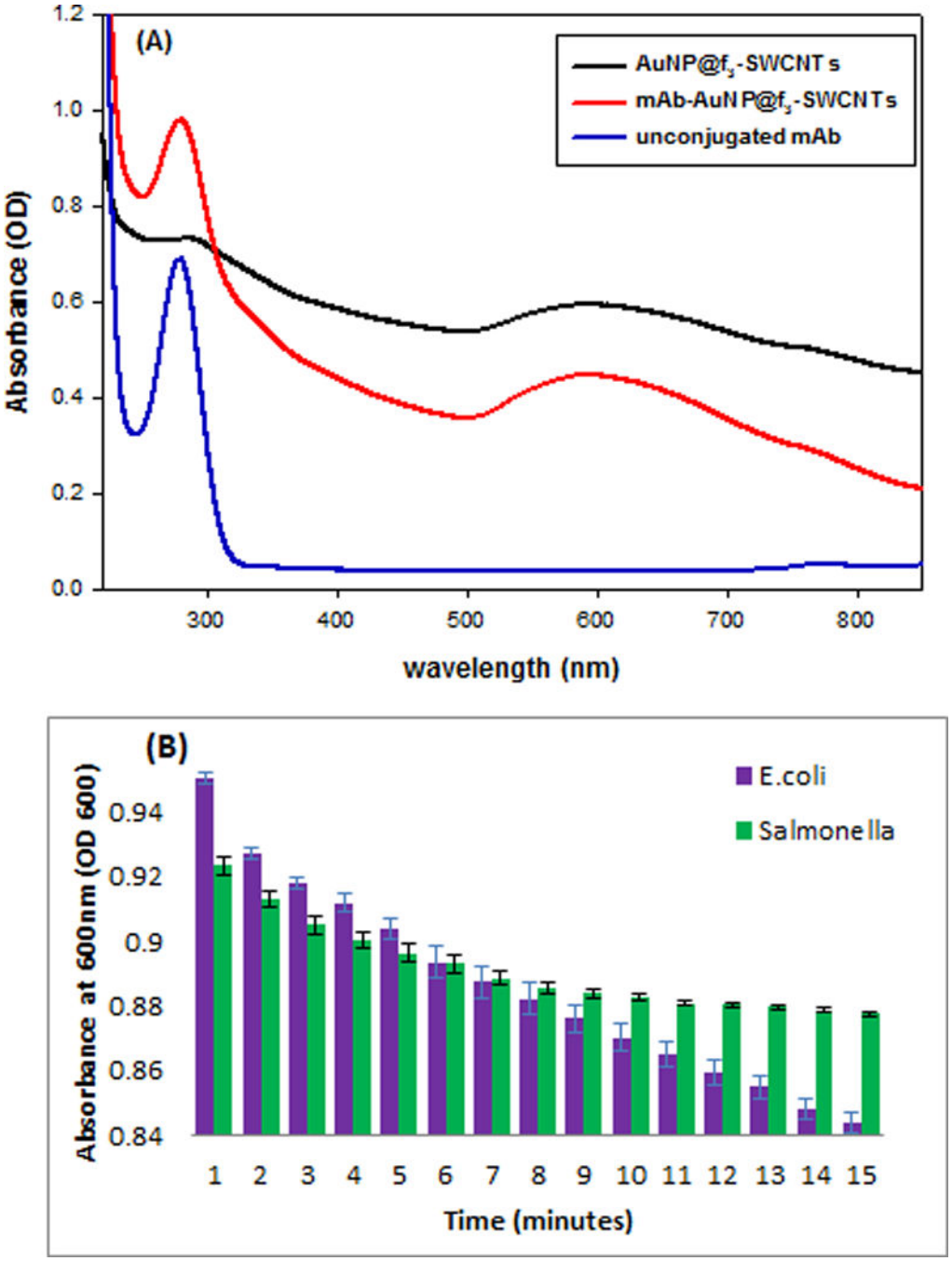

Figure 5.

(A) UV-Vis absorbance spectra of unconjugated antibody (blue curve), AuNP@f_3-SWCNTs (black curve) and antibody conjugated-AuNP@f_3-SWCNTs (red curve). (B) Bacterial capturing selectivity of the antibody conjugated-AuNP@f_3-SWCNT represented by absorbance at OD_{600} for E .coli (purple bars) and Salmonella DT104 (green bars). Error bars show the standard deviation (SD) of three measurements.

NIH-PA Author Manuscript
NIH-PA Author Manuscript
NIH-PA Author Manuscript

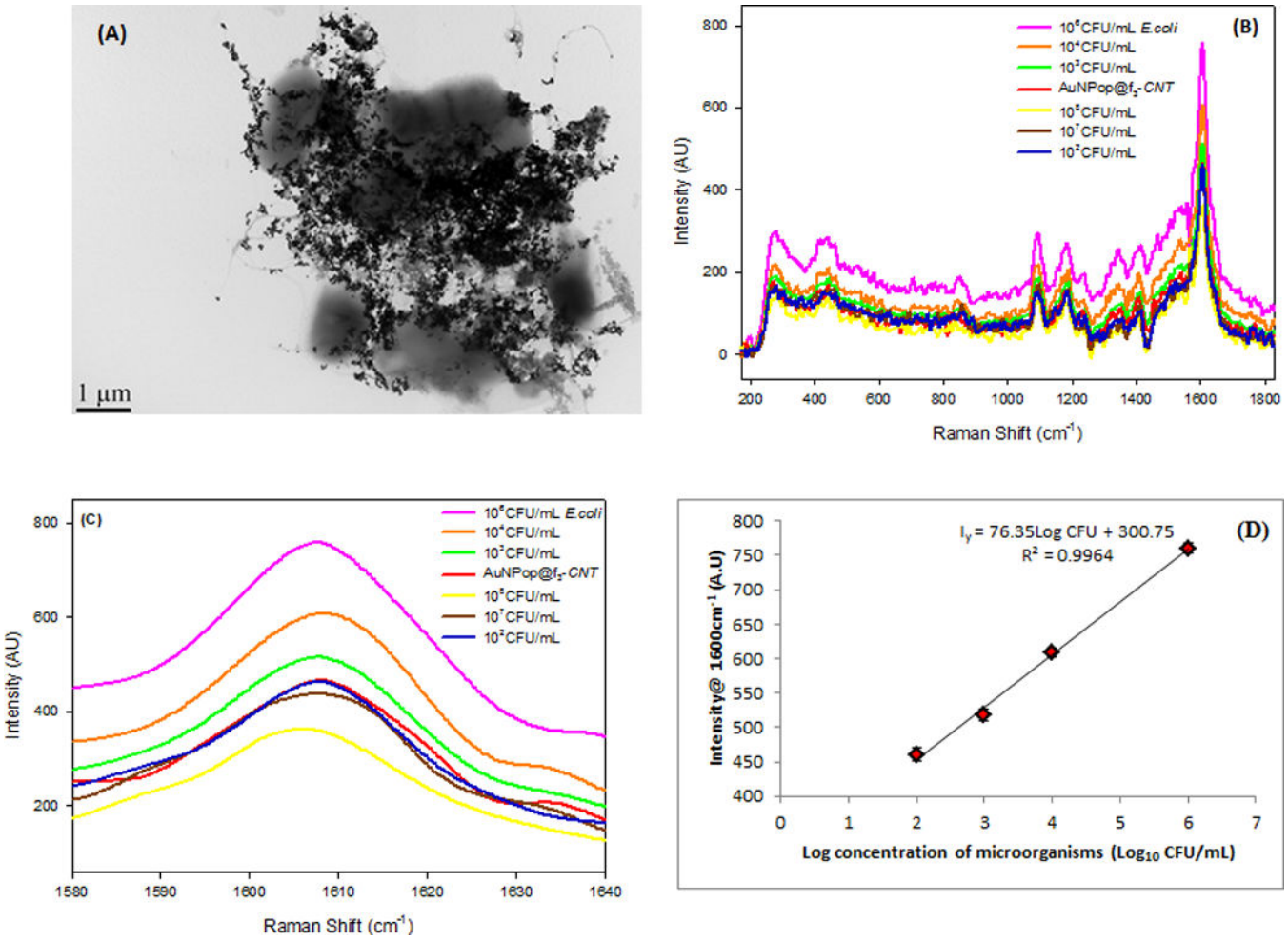

Figure 6.

(A) TEM image shows immobilization of *E. coli* by mAb-AuNP@f_3-SWCNTs hybrid nanomaterial (B) SERS response of the hybrid nanomaterial at different dilutions of *E. coli* at 670 nm excitation (C) High resolution SERS spectral region between 1580–1640 cm^{-1} showing the dependence of G-band intensity on concentration of micro-organisms and limit of detection of 10^2 CFU/mL (D) A plot showing the linear relationship between the peak intensity of the G-band at ~1600 cm^{-1} and the Log concentration of the microorganism. The linearity fails at concentrations ≥10^7 CFU/mL (black and yellow curves). Error bars show the standard deviation (SD) of three measurements.

NIH-PA Author Manuscript
NIH-PA Author Manuscript
NIH-PA Author Manuscript

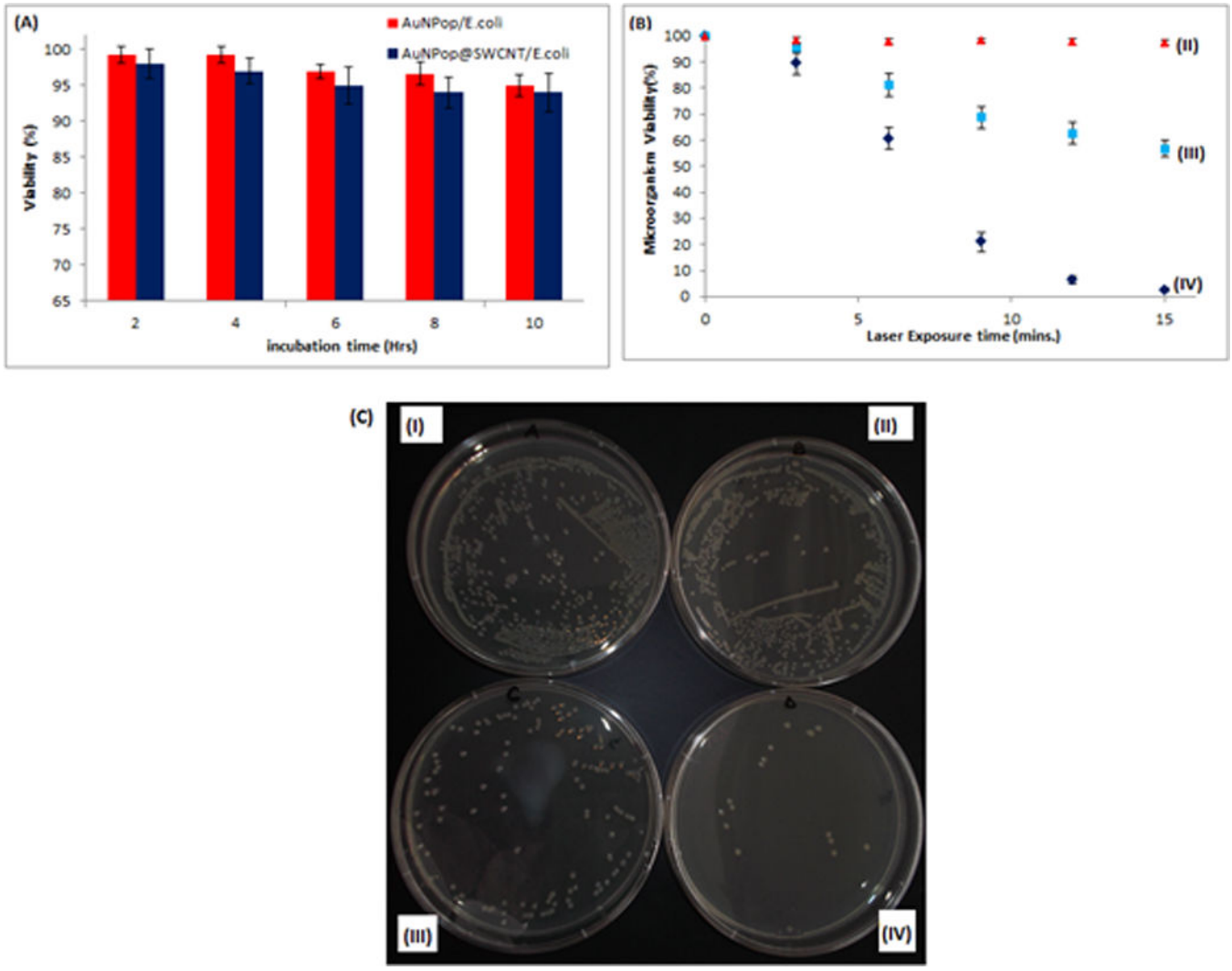

Figure 7.

(A) Histogram demonstrating non-toxicity of AuNP@f_3-SWCNT and AuNPs in *E. coli* incubated after different times. (B)Scatter plot showing viability (%) of *E. coli* when exposed to 670 nm laser at 1.5–2.5 W/cm^2 for 15 minutes: (II) Untreated *E. coli* (III) *E. coli* immobilized onto mAb conjugated AuNPs and (IV) *E. coli* immobilized onto mAb-AuNP@f_3-SWCNT (C) Digital photographs of colonies of *E. coli* grown on Luria Bertani Agar plates obtained from 15 minutes of exposure to 670 nm laser at 1.5–2.5 W/cm^2 (II-IV), (II) *E. coli* sample, (III) *E. coli* immobilized onto mAb conjugated Au NPs and (IV) *E. coli* immobilized onto mAb-AuNPop@f_3-SWCNT. (I) Unexposed *E. coli* immobilized onto mAb-AuNP@f_3-SWCNT.

NIH-PA Author Manuscript

NIH-PA Author Manuscript

NIH-PA Author Manuscript

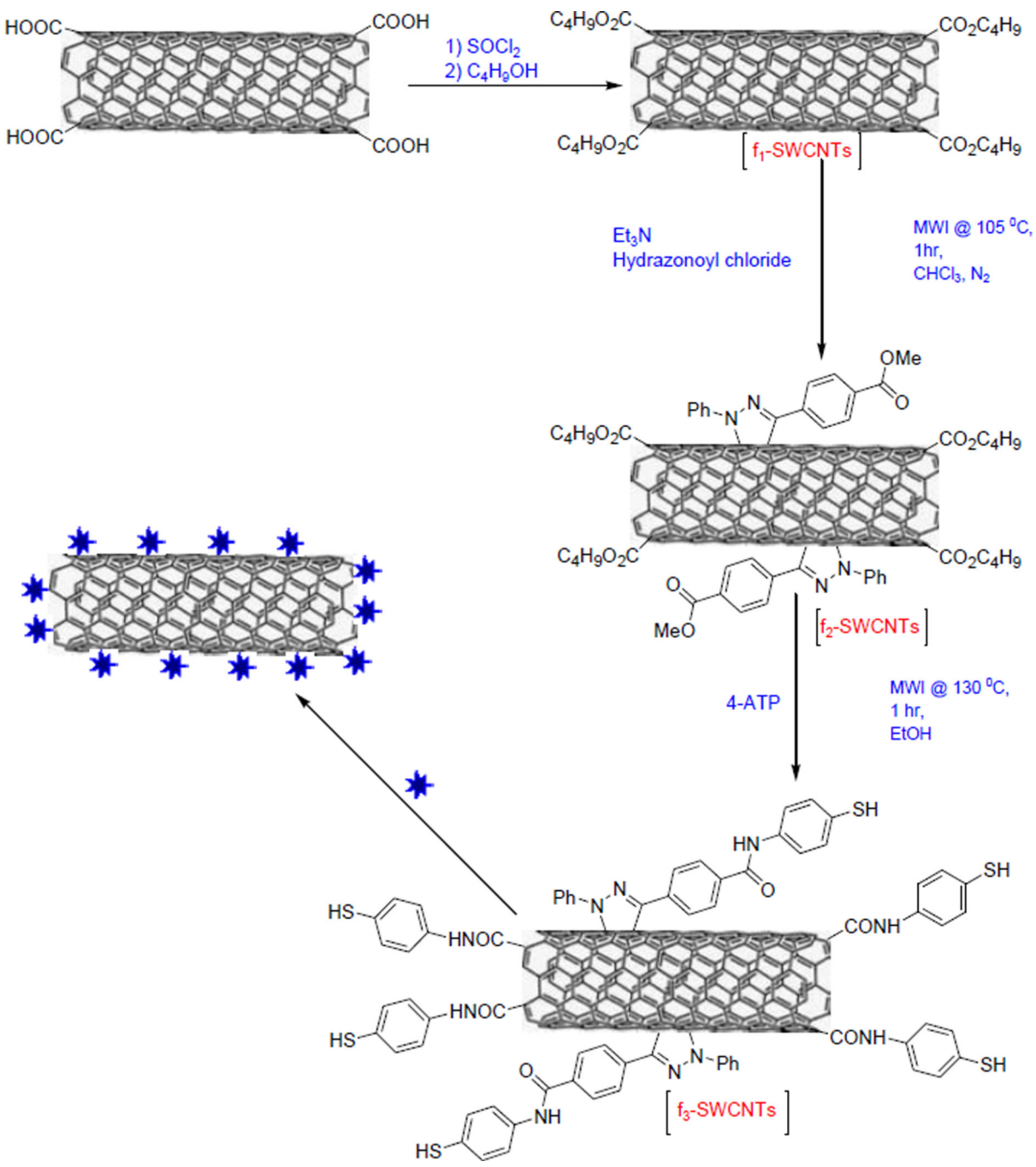

Scheme 1.

Microwave-promoted 1,3-dipolar cycloaddition and amidation of the ester-modified SWCNTs and attachment of the Gold nanopopcorns.